Mechanical, thermal and physical properties of new chloroantimonite glasses in the Sb2O3 -PbCl 2 -AgCl system

Djamel Yezli, Messaoud Legouera, Rochdi El Abdi, Marcel Poulain, Vincent Burgaud

Mechanical, thermal and physical properties of new chloroantimonite glasses in the Sb_2O_3-$PbCl_2$-AgCl system

Djamel Yezli [a], Messaoud Legouera [a], Rochdi El Abdi [b, *], Marcel Poulain [c], Vincent Burgaud [b]

[a] Département de Génie Mécanique, Université du 20 aout 1955, Skikda 21000, Algérie.
[b] IPR, Département Mécanique &Verres, Université de Rennes1, 35042 Rennes cedex, France.
[c] UMR Sciences Chimiques, Université de Rennes1, 35042 Rennes cedex, France.
*E-mail : relabdi@univ-rennes1.fr ; Tel & Fax : +33 (0) 2 23 23 41 12

ABSTRACT
New chloroantimonite glasses have been obtained in the Sb_2O_3-$PbCl_2$-AgCl ternary system. Thermal, optical and mechanical properties have been studied. The silver chloride concentration was increased at the expense of antimony oxide according to the following composition rules: $(80-x)Sb_2O_3$-$20PbCl_2$-$xAgCl$; $(70-x)Sb_2O_3$-$30PbCl_2$-$xAgCl$.
Depending on AgCl content, Vickers micro-hardness varies between 110 and 140 MPa. Elastic moduli have been measured by ultrasonic velocity. Optical transmission range extends from 400 nm in the visible spectrum to 7 μm in the infrared. Refractive index is close to 2. Glass transition temperature measured by DSC ranges from 250 °C to 290 °C. The influence of silver and lead chloride on physical properties was discussed.

***Keywords**: Chloro-antimonite glasses, Optical properties, Mechanical properties, Glass transition temperature, Heat flow.*

1. Introduction

Glass forming ability of antimony sesquioxide Sb_2O_3 has been predicted by Zachariasen [1] and confirmed by several authors [2, 3]. While vitreous Sb_2O_3 has been reported, multicomponent glasses have been characterized either in pure oxides systems or in oxyhalide [4-7] and oxysulphide systems [8]. Not surprisingly, large Sb_2O_3 amounts could be incorporated in silicates and phosphate glasses [9-11]. Antimonite glasses free of classical vitrifyers appear attractive for their extended infrared transmission range [3, 5, 8] and their large refractive index (> 2) [5] and their non linear optical properties [12-13]. In this respect they compare to tellurite glasses that have been largely studied. The chlorides of the metal halide may be incorporated into the glasses of heavy oxides to obtain a very large subfamily [5]. This work is centred upon new chloro-antimonite glasses associating antimony oxide and

lead and silver halides. Following the pioneering work of Dubois and Portier [5], numerous glass forming systems have been reported [14-18]. While alkali antimonite glasses have been studied [3, 15], more numerous and more stable glasses were identified, especially by incorporating a third component in the binary Sb_2O_3 – $PbCl_2$ glass.

In this paper we focus on the optical and mechanical properties of glasses in the Sb_2O_3 – $PbCl_2$ – AgCl ternary system.

2. Experimental

2.1. Glass synthesis

Chemical reagents used for this study were Sb_2O_3 99.9 % Acros organics, $PbCl_2$ 99 %+ form Hichem and AgCl 99.9 % from Alfa Aesar.
Main physical properties of these starting materials were given in Table 1.

Table 1
Mechanical properties of used materials.

Components	**Density** (g/cm^3)	**Molar weight** (g/mol.)	**Vickers hardness** (N/mm^2)	**Molar volume** (cm^3/mol.)
$PbCl_2$	5.7	278.1	138-140	48.78
AgCl	5.4	143.32	10-12	26.54
Sb_2O_3	5.75	291.4	65-68	50.79

Glass preparation was carried out using the classical processing steps of melting, fining, cooling, casting and annealing. The calculated amount of starting materials was thoroughly mixed in an agate mortar, and then introduced in a silica tube. Silica was not an ideal material for this glass synthesis as it slowly reacts with glass melt. However it makes a better choice than platinum or gold that may form alloys if oxido-reduction reactions result in metallic particles. In this case, crucible was destroyed.
After melting, fining was achieved at room atmosphere around 850 °C. Then melt is rapidly cooled down around 600 °C and poured onto a brass mould preheated at 250 °C, that was around glass transition temperature Tg. After solidification, sample was set in an oven at Tg

for the thermal homogenization the removal of the thermally induced stressed. After a few hours, oven was set off to ensure homogenous cooling.

2.2. Physical measurements

Characteristic temperatures – Tg for glass transition, Tx for onset of crystallization, and Tc for exotherm maximum were measured by differential scanning calorimetry using a DSC Q20 set-up from TA instruments.

Density was measured by Archimedean method using CCl_4 as a buoying liquid. Molar volume was calculated from the following relation [19]:

$$V = \sum x_i.M_i / d \quad (1)$$

where x_i is the molar fraction of the *i* element, M_i is the molar weight of the *i* element and *d* is material density. The molar weight of the glass M_g is expressed as $M_g = \sum x_i.M_i$; it depends directly on the chemical formulation.

Microhardness was measured using a Matuzawa Vmt 75 set-up with 50 N loading charge and 10 seconds indentation time.

Elastic moduli were measured by ultrasonic velocity using a "Parametric 5800" and an oscilloscope "model 54502".

Optical transmission has been recorded in the UV-visible range using a Perkin Elmer spectrophotometer between 300 nm and 3000 nm. For infrared transmission a Bruker Tensor 37 Fourier transformed spectrometer was used between 400 cm^{-1} and 4000 cm^{-1}.

3. Results and discussion

3.1 Glass formation

The starting point of our study was the binary glass Sb_2O_3-$PbCl_2$ reported by Dubois and *al* [5]. A third component has been added to form a ternary system. The glass forming area in this system was drawn at Fig. 1. The limits of the vitreous domain correspond to small spheres, roughly 1 mm in diameter. Larger and thicker samples could be obtained for the non limiting composition. Antimony oxide was the main component while $PbCl_2$ concentration does not exceed 40 mol % and maximum AgCl content is less than 30 mol %. Note that no binary glass was observed in the Sb_2O_3-AgCl system. The vitreous state was assessed by

visual inspection and confirmed by thermal analysis. Samples of several millimeters in thickness were prepared for optical and mechanical measurements. It appears that the most stable compositions correspond to the 20% molar concentration of lead chloride.

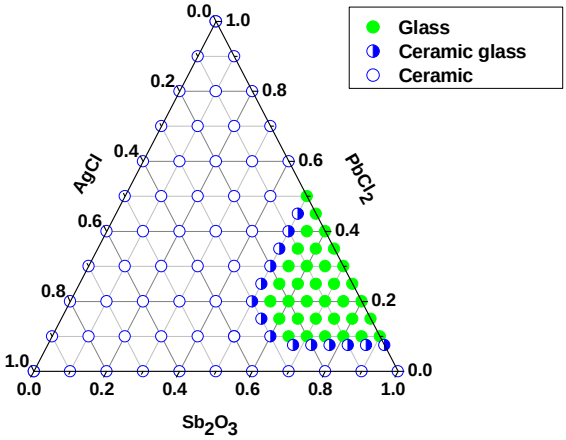

Fig. 1. Compositional limits for glass formation in Sb_2O_3-$PbCl_2$-$AgCl_2$ system.

3.2. Density and molar volume

Density has been measured for two series of glasses defined by the following composition rules: (80-x)Sb_2O_3-20$PbCl_2$-x$AgCl$ and (70-x)Sb_2O_3-30$PbCl_2$-x$AgCl$.

This corresponds to the substitution of Sb_2O_3 by AgCl. Collected data provide information on the influence of silver chloride on physical properties. Figure 2 (a, b) reports the changes of density and molar volume versus AgCl concentration.

Both density and molar volume decreased as AgCl replaces Sb_2O_3. The molar weight corresponds to the chemical formula: (α Sb_2O_3 - β $PbCl_2$ - γ $AgCl$) with $\alpha + \beta + \gamma = 100$.

The density was measured for the two series of glasses, which makes it possible to evaluate the influence of the composition. The influence of Sb / Ag on density values is illustrated by Fig. 2 (a, b). For each curve, the lead chloride content was kept constant. The density decrease resulting from the Sb/Ag substitution could be expected insofar as Ag^+ ion is larger and lighter than Sb^{3+}, while chlorine anions are also larger than oxygen anions. This results in a smaller number of ions per unit volume. The conjugation of these two factors – size and atomic weight- accounts for density reduction.

Our measurements allow comparing glasses with 20 % and 30 mol % lead chloride, corresponding to the substitution of antimony oxide by lead chloride. Density increases with lead concentration. In this case the predominant factor is atomic weight: divalent lead Pb^{2+} is

much heavier than Sb^{3+}. This appears clearly in Figs. 2. Density and molar volume follow almost quasi-linear slopes especially for ((70-x) Sb_2O_3- 30$PbCl_2$ –xAgCl) system.

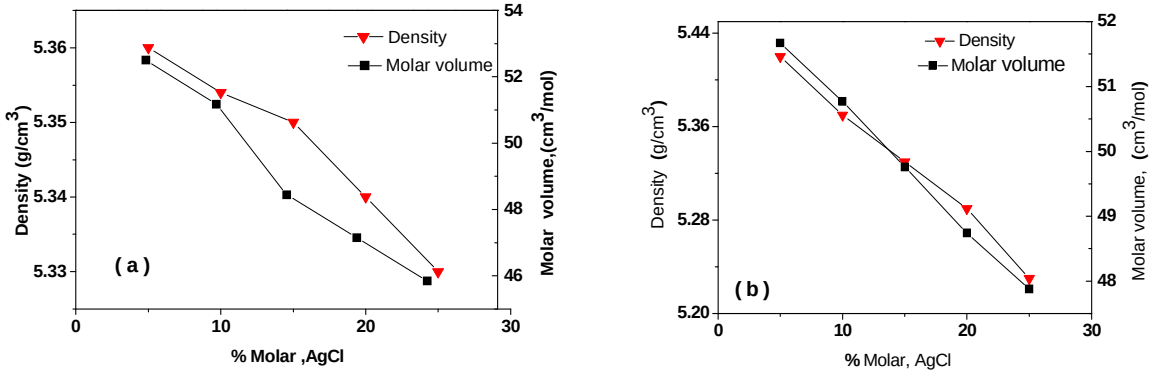

Fig. 2. Evolution of the density and molar volume based on AgCl; (a): ((80-x)Sb_2O_3 -20$PbCl_2$-xAgCl) (b): ((70-x) Sb_2O_3- 30$PbCl_2$ –xAgCl) system.

3.3. Thermal properties

The characteristic temperatures of the selected glasses have been measured. They include temperatures of glass transition Tg, onset of crystallization Tx and exothermic maximum Tc.

The Tx-Tg difference makes a qualitative criterion of the stability versus devitrification. Their variation as a function of AgCl concentration is drawn in Fig. 3 (a, b). The general trend was that Tg decreases as AgCl substitutes Sb_2O_3. This substitution increases the Cl/O ratio. As the AgCl bond was weaker than the Sb-O bond, the resistance to thermal motion decreases and consequently Tg was smaller.

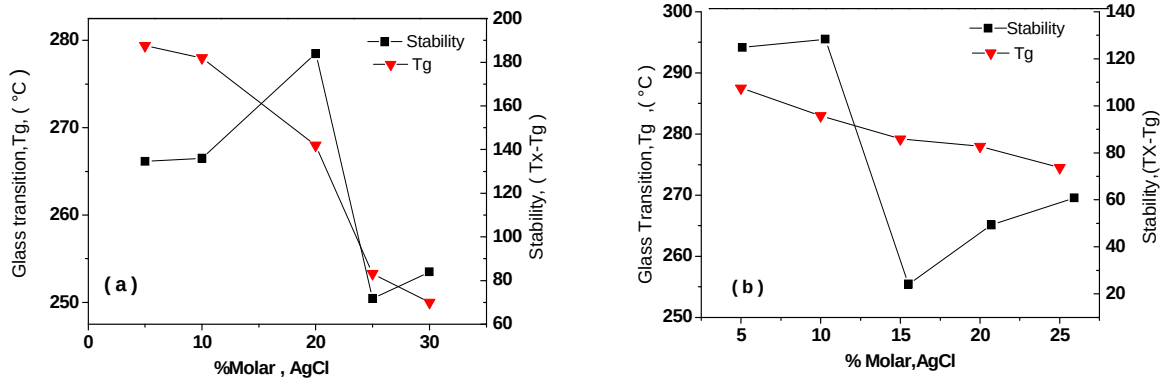

Fig. 3. Evolution of the Tg and stability based on AgCl of (a): ((80-x)Sb_2O_3-20$PbCl_2$-xAgCl); (b): ((70-x) Sb_2O_3-30$PbCl_2$-xAgCl) system

Table 2 gives the detailed composition of the studied glass samples.

The DSC scans of Fig. 4 suggest that glasses far from the limiting compositions were very stable insofar as crystallization peak is hardly visible at the DSC heating rate (20K/min).

Table 2
Composition of samples studied

Samples	**(80-x)Sb_2O_3-20$PbCl_2$-xAgCl**
D1	75Sb_2O_3-20$PbCl_2$-5AgCl
D2	70Sb_2O_3-20$PbCl_2$-10AgCl
D3	60Sb_2O_3-20$PbCl_2$-20AgCl
D4	55Sb_2O_3-20$PbCl_2$-25AgCl
D5	50Sb_2O_3-20$PbCl_2$-30AgCl
	(70-x)Sb_2O_3-30$PbCl_2$-xAgCl
E1	65Sb_2O_3-30$PbCl_2$-5AgCl
E2	60Sb_2O_3-30$PbCl_2$-10AgCl
E3	55Sb_2O_3-30$PbCl_2$-15AgCl
E4	50Sb_2O_3-30$PbCl_2$-20AgCl
E5	45Sb_2O_3-30$PbCl_2$-25AgCl

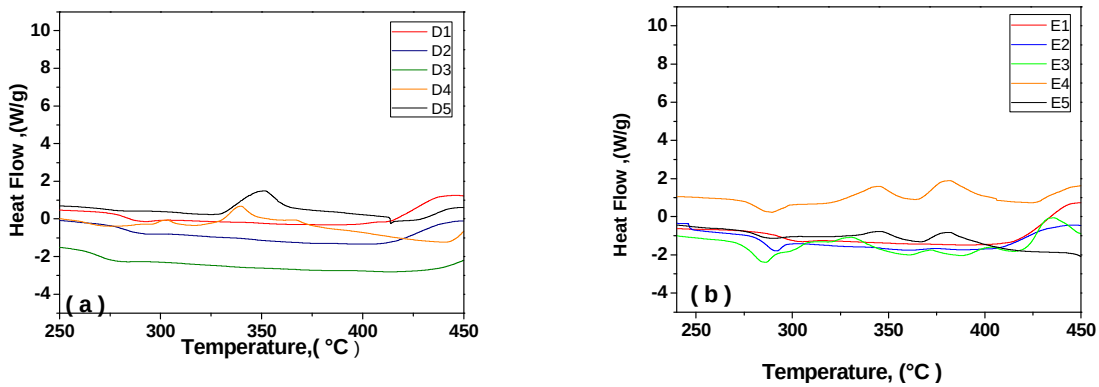

Fig. 4. DSC curves for (a): (80-x)Sb_2O_3-20$PbCl_2$-xAgCl; (b): (70-x) Sb_2O_3-30$PbCl_2$-xAgCl system.

3.4. Vickers micro-hardness and Young's modulus

To characterize the hardness and the deformation mode of the glass surface, the indentation hardness technique was used. When a sharp indenter, such as the Vickers indenter, was loaded onto a material, a residual surface impression was observed after unloading, and the material hardness was generally estimated from the projected area of the impression. The deformation was dependent on the applied load, the temperature and the load time.

Indentation experiments were performed with a Vickers diamond indenter. Vickers diamond pyramid hardness was determined in practice by measuring the diagonal length of the indentation produced by the penetration of a square-based pyramid having an angle of 136° between opposite pyramid faces. The hardness number *HV* was given by the equation:

$$HV = \frac{0.1891\ F}{d^2} \qquad \text{(in N/mm}^2\text{)} \qquad (2)$$

F is the applied load, and *d* the average length of the square diagonal which is left by the indenter.

Although the diagonal *d*, in Eq. (2) was obtained by measurement after the removal of the load, it was known that the change in the lengths of the diagonals upon unloading was very small [20] and almost insignificant when compared to the diagonal length itself.

The Vickers hardness was calculated for each sample using the average residual area of 9 indentations.

The micro-hardness was measured for the two sample systems as shown in Fig. 5 (a, b). For the studied glasses, the initial hardness value was approximately equal to 140 N/mm^2 and decreases according to AgCl concentration (AgCl has the lower hardness value between 10 and 12 N/mm^2 (Table1)). This decreasing can reach 22% and the insertion of more and more AgCl into the glasses network leads to a decreasing of the link forces between different atoms. The micro hardness was also connected to the dilatometric softening point. The glass micro-hardness systematically decreases according to the softening temperature which depends on the transition glass temperature Tg. Thus, the evolution of micro-hardness and the one of the transition glass temperature were similar.

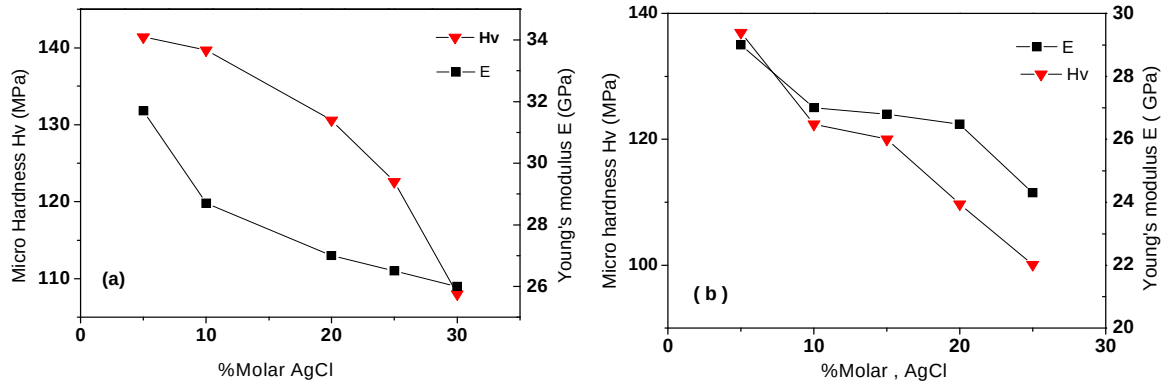

Fig. 5. Evolution of the micro-hardness (Hv) and Young's modulus (E) based on AgCl, a: ((80-x)Sb_2O_3-20$PbCl_2$-xAgCl); (b): ((70-x)Sb_2O_3-30$PbCl_2$-xAgCl) system

3.5. Flaking

Tenacity represents the resistance of the material against the defects or cracks propagation. It was expressed in MPa $\sqrt{m}$.

Figures below show that when the percentage of $PbCl_2$ increases, the tenacity of the glass increases. Indeed, in the above figure Fig.6 (a, b), radial cracks are visible and start from the top of each corner of the Vickers indenter footprint. These cracks have a size between 1 and 2 mm.

The increase of $PbCl_2$ concentration (rising from 20 to 30%) makes the tough material and radial cracks have disappeared (Fig. 6, c, d).

$PbCl_2$ (which has the highest Vickers hardness than the two other components of the studied glasses) leads to higher overall hardness when its concentration increases. This has the effect of producing glass flakes which overlap towards a small thickness of the sample and which appear on either side of the footprint of the diamond indentor.

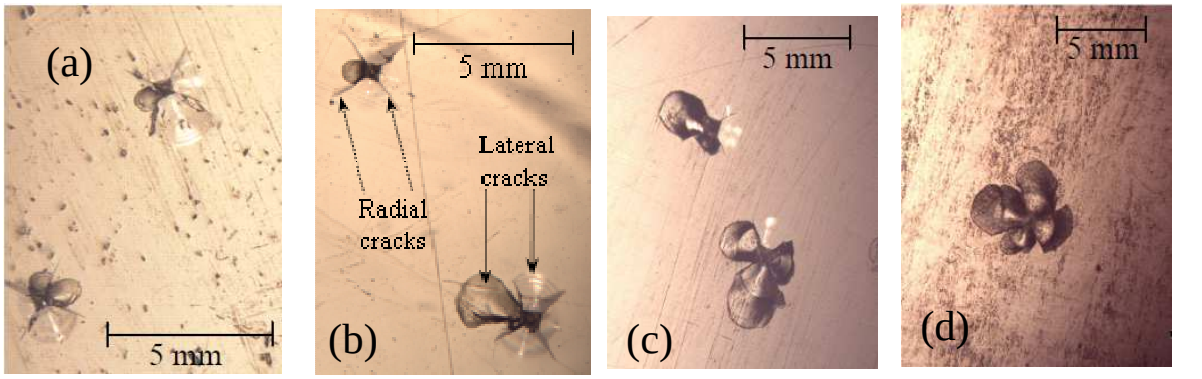

$75Sb_2O_3$-$20PbCl_2$-5AgCl	$70Sb_2O_3$-$20PbCl_2$-10AgCl	$50Sb_2O_3$-$30PbCl_2$-20AgCl	$45Sb_2O_3$-$30PbCl_2$-25AgCl

Fig. 6. Radial and lateral cracks for different $PbCl_2$ molar concentrations

3.6. Infrared and UV transmission

Fig. 7 shows the visible Ultra-violet transmission spectrum. Perkin Elmer spectrophotometer was used and the sample thickness was equal to 2 mm. The level of the maximum transmission (about 75%) was due to a high refractive index greater than 2, which causes reflection losses. The base line of E glass sample (Fig.7) is shifted towards smaller transmission value because it contains physical defects that result in high scattering losses.

The yellow color of antimony glasses reflects their limited ultraviolet transmission below 400 nm and partial blue absorption. This is due to the low gap band of the free electron pair of Sb (III).

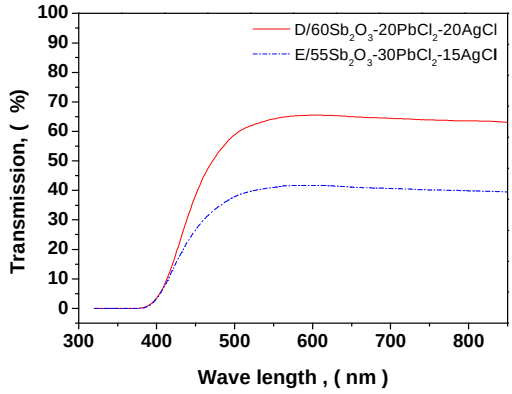

Fig. 7. Ultra-violet transmission spectrum

In these glasses, infrared transmission is limited by chemical bonds vibrations and their harmonics that create the multi phonon absorption edge.

A Bruker Tensor 37 Fourier transformed spectrometer was used for measurement of infrared transmission (2.5 to 25 µm) with samples of 2 mm thickness with parallel plane sections. Fig. 8 gives IR transmission for two samples of the studied systems.

The main extrinsic absorption bands in these antimonite glasses are due to hydroxyls OH (3300 cm^{-1}), to Si-O bonds (1800 cm^{-1}) or to carbon dioxide (2400 cm^{-1}).

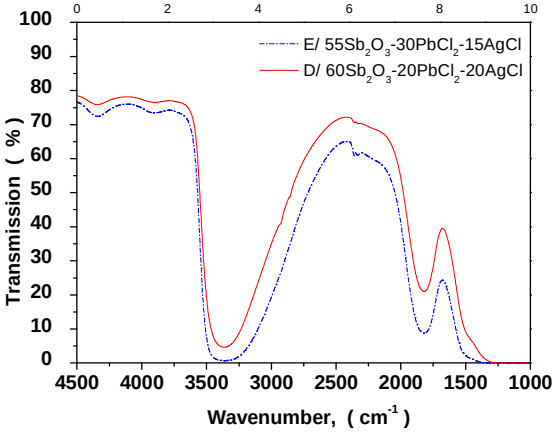

Fig. 8. Infrared transmission spectrum.

4. Conclusion

Glass formation has been studied in the Sb_2O_3-$PbCl_2$-AgCl ternary system. In this system two groups of glasses were prepared according to the following composition rules:

(80-x) Sb_2O_3-20$PbCl_2$-xAgCl and (70-x) Sb_2O_3-30$PbCl_2$-xAgCl.

The increase of AgCl molar concentration leads to the decrease of the molar volume and the glass density. But increasing $PbCl_2$ concentration has the reverse effect. Similar variations are observed for the transition glass temperature according to AgCl and $PbCl_2$ concentrations. A practical observation was that the more stable system was with 20% of $PbCl_2$ in the ((80-x) Sb_2O_3-20$PbCl_2$-xAgCl) series.

Young modulus and micro-hardness behave in the same way and both decrease when the AgCl concentration increases. The larger values of hardness and Young's modulus were obtained in the previous system ((80-x) Sb_2O_3-20$PbCl_2$-xAgCl), and the maximum is obtained for 5% AgCl concentration.

Finally, this study showed the interest of AgCl which can lead to optimized glasses for various applications.

References

[1] W. H. Zachariasen, J. Chem. Soc. 54 (1932) 3841- 3851.

[2] A. Winter, J. Am. Ceram. Soc. 40 (1957) 54-58.

[3] A. Winter, Verres réfractaires, 36 (1982) 353-376

[4] J. F. Bednarik, J. A. Neely, Glass Tech. Ber 55 (1982) 126-129.

[5] B. Dubois, H. Aomi, J. J. Videau, J. Portier, P. Haggenmuller, Mater. Res. Bull. 19 (1984) 1317-1323.

[6] M. R. Sahar, M. M. Ahmed, D. Holland, Phys. Chem. Glasses 31 (1990) 126-131.

[7] M. R. Sahar, D. Holland, J. Non-Cryst. Solids 140 (1992) 107-111.

[8] L. Zan, J. S. Zhong, Q. R. Luo, J. Non-Cryst. Solids 256-257 (1999), 396-399.

[9] A. Datta, A. K. Giri, D. Chakravorty, Physic. Rev. B 47 (1993) 16242- 16246

[10] B.V. R. Chowdari, S. K. Akhter, Solid State Ionics 25 (1987) 109-119.

[11] S. K. Akhter, Solid State Ionics 51 (1992) 305-310.

[12] J. S. Wang, E. E. Vogel, E. Snitzer, Opt. Mater. 3 (1994) 187-203.

[13] R. E. De Araujo, C.B. De Araujo, G. Poirier, M. Poulain, Y. Messaddeq, Appl. Phys. Lett. 81 (2002) 4694-4696.

[14] G. Poirier, M. A. Poulain, M. J. Poulain, J. Non-Cryst. Solids 284 (2001) 117-122.

[15] M.T. Soltani, A. Boutarfaia, R. Makhloufi, M. Poulain, J. Phys. Chem. Solids 64 (2003) 2307- 2312.

[16] M. Legouera, P. Kostka, M. Poulain, J. Phys. Chem. Solids 65 (2004) 901-906

[17] M. T. Soltani, T. Djouama, A. Boutarfaia, M. Poulain, J. Optoelectron. Advanced Mater. Symposia 1 (2009) 339-342

[18] M. Iezid, M. Legouera, F. Goumeindane, M. Poulain, V. Nazabal, R. Lebullenger, J. Non-Cryst Solids 357 (2011) 2984-2988.

[19] J. M. Stevels, Progress in the theory of the physical properties of glasses, Elsevier, New York, 1948, 96.

[20] M. Petzold, J. Landgraf, M. Füting, J. M. Olaf, Thin Sol. Films 264 (1995) 153-158.